AD-A042 323 NAVAL POSTGRADUATE SCHOOL MONTEREY CALIF F/G 7/4
LASER INDUCED DESORPTION OF GAS FROM STAINLESS STEEL SURFACES.(U)
JUN 77 J S POLK

UNCLASSIFIED NL

1 OF 1
ADA042323

END

DATE FILMED
8-77

(2)

NAVAL POSTGRADUATE SCHOOL
Monterey, California

THESIS

LASER INDUCED DESORPTION OF GAS

FROM STAINLESS STEEL SURFACES

by

James Stanley Polk

June 1977

Thesis Advisor: F. R. Schwirzke

Approved for public release; distribution unlimited.

UNCLASSIFIED

SECURITY CLASSIFICATION OF THIS PAGE (When Data Entered)

REPORT DOCUMENTATION PAGE

READ INSTRUCTIONS BEFORE COMPLETING FORM

1. REPORT NUMBER	2. GOVT ACCESSION NO.
3. RECIPIENT'S CATALOG NUMBER (9)	
4. TITLE (and Subtitle) (6) Laser Induced Desorption of Gas from Stainless Steel Surfaces.	5. TYPE OF REPORT & PERIOD COVERED Master's Thesis, June 1977
	6. PERFORMING ORG. REPORT NUMBER
7. AUTHOR(s) (10) James Stanley Polk	8. CONTRACT OR GRANT NUMBER(s)
9. PERFORMING ORGANIZATION NAME AND ADDRESS Naval Postgraduate School Monterey, California 93940	10. PROGRAM ELEMENT, PROJECT, TASK AREA & WORK UNIT NUMBERS
11. CONTROLLING OFFICE NAME AND ADDRESS (11) Naval Postgraduate School Monterey, California 93940	12. REPORT DATE June 1977
	13. NUMBER OF PAGES 67
14. MONITORING AGENCY NAME & ADDRESS (if different from Controlling Office) Naval Postgraduate School Monterey, California 93940 (12) 67 p.	15. SECURITY CLASS. (of this report) UNCLASSIFIED
	15a. DECLASSIFICATION/DOWNGRADING SCHEDULE

16. DISTRIBUTION STATEMENT (of this Report)

Approved for public release; distribution unlimited

17. DISTRIBUTION STATEMENT (of the abstract entered in Block 20, if different from Report)

18. SUPPLEMENTARY NOTES

19. KEY WORDS (Continue on reverse side if necessary and identify by block number)

Laser Induced desorption

10 to the -7th power

20. ABSTRACT (Continue on reverse side if necessary and identify by block number)

Laser induced desorption of gases from stainless steel target surfaces in vacuum of the order of 10^{-7} Torr was studied as a special case of photon-induced desorption. Adsorption phenomena and induced desorption were examined with emphasis on desorption caused by direct photon excitation and photon-induced thermal effects. The photon sources employed were infrared laser pulses with intensities of the order of 10 MW/cm^2 produced by a Q-switched Nd-glass laser. Total pressure and mass spectrometric partial

DD FORM 1 JAN 73 1473 EDITION OF 1 NOV 65 IS OBSOLETE S/N 0102-014-6601 |

UNCLASSIFIED

SECURITY CLASSIFICATION OF THIS PAGE (When Data Entered)

251450

pressure measurements of hydrogen, carbon dioxide, and nitrogen/carbon monoxide were taken. The results indicated that laser induced desorption is principally a thermal mechanism. Desorption energies derived from measured partial pressure changes and calculated surface temperature increases were found to be 8.5 kcal/mole for hydrogen and 14.7 kcal/mole for carbon dioxide.

Approved for public release; distribution unlimited.

Laser Induced Desorption of Gas from Stainless Steel Surfaces

by

James Stanley Polk
Lieutenant-Commander, United States Navy
B.A., University of Notre Dame, 1967
B.S.C.E., University of Notre Dame, 1968

Submitted in partial fulfillment of the requirements for the degree of

MASTER OF SCIENCE IN PHYSICS

from the

NAVAL POSTGRADUATE SCHOOL

June 1977

Author: James Stanley Polk

Approved by: Fred Schwirzke
Thesis Advisor

R.W. Cooper
Second Reader

U.E. Kelly
Chairman, Department of Physics and Chemistry

R.W. Fossum
Dean of Science and Engineering

ABSTRACT

Laser induced desorption of gases from stainless steel target surfaces in vacuum of the order of 10^{-7} Torr was studied as a special case of photon-induced desorption. Adsorption phenomena and induced desorption were examined with emphasis on desorption caused by direct photon excitation and by photon-induced thermal effects. The photon sources employed were infrared laser pulses with intensities of the order of 10 MW/cm^2 produced by a Q-switched Nd-glass laser. Total pressure and mass spectrometric partial pressure measurements of hydrogen, carbon dioxide, and nitrogen/carbon monoxide were taken. The results indicated that laser induced desorption is principally a thermal mechanism. Desorption energies derived from measured partial pressure changes and calculated surface temperature increases were found to be 8.5 kcal/mole for hydrogen and 14.7 kcal/mole for carbon dioxide.

TABLE OF CONTENTS

LIST OF FIGURES

ACKNOWLEDGEMENT

I wish to thank technicians Robert Sanders and Thomas Maris for their assistance in calibrating, repairing and maintaining all equipment needed to obtain data for this thesis. Without their constant attention and prompt reaction to hardware problems, this thesis could not have been completed in the alloted time. I should also like to extend my sincere gratitude to Professor Schwirzke for his help and guidance throughout the experiment and for his constructive co[illegible]nts during the report writing. Finally, I [illegible] to thank my lab partner and fellow student, Maj. [illegible]" Halliday, C.F., for all of his physical labor, common sense suggestions, and morale sustaining contributions to the day to day effort involved in preparing this thesis.

I. INTRODUCTION

The interactions between a solid surface and a gaseous environment take place in a narrow interface region only a few angstroms wide. The details of these interactions are not well understood. By inducing the desorption of gas from solid surfaces and analyzing the desorbed species, information regarding the nature of the solid-gas interface interactions can be obtained [1].

Induced desorption may also be used as a means of cleaning a surface. Clean surfaces are important in many areas of modern technology. Many surface physics experiments require atomically clean surfaces which are difficult to obtain in the best vacuum systems. The properties of microelectronic semiconductor elements with high surface area to bulk volume ratios can be greatly affected by adsorbed gas layers. Contamination of plasmas by release of gas from the walls of containment vessels is a severe problem in experiments leading to fusion reactions.

Photon-induced desorption has several advantages over other methods for inducing desorption. No foreign atoms or ions are introduced into the interface region. Electrically neutral photons reduce requirements for complex electric control fields. Migration of impurities to the surface due to bulk heating of a sample is eliminated. Photons can be introduced into a vacuum system through an optically transparent window without spoiling the vacuum [2,3].

Despite the above advantages, this method has not been as widely used as other methods. One of the reasons for

this has been the lack of convenient, controllable sources. Modern laser developments have produced much improved directional, coherent, and monochromatic photon sources. Improved lasers should prove to be useful desorption tools.

Various facets of photon induced desorption from solid surfaces have been explored. The release of gases from metal surfaces under vacuum conditions caused by photons in the visible and ultraviolet regions has been reported [4,5,6]. Q-switched ruby laser pulses have also been used to induce desorption from metal and semiconductor surfaces [2,7,8]. It has been shown that the impact of a rapidly expanding laser generated plasma cloud on the surfaces of a vacuum chamber can result in the release of a relatively large amount of adsorbed gas [9]. Mass spectrometric studies of gases released by X-ray radiation of stainless steel surfaces have also been reported [10].

It was the purpose of this study to investigate gas release from stainless steel surfaces irradiated by infrared laser pulses. Both total pressure and mass spectrometric measurements were employed. The incident intensities were below the level which would cause the solid surface to melt or vaporize. There were two reasons for using these low intensities. First, large changes in the physical properties of the surface region were minimized. Second, gas desorption from the chamber walls caused by the impact of a laser-generated plasma cloud was avoided. Thus only the desorption effects due to direct photon excitation and to photon-induced heating needed to be considered.

II. BACKGROUND

A. DEFINITIONS

1. Adsorption

In an equilibrium situation between a solid and a gas, a higher concentration of gas will be found at the surface of the solid than in the free gas. This phenomenon is called adsorption. Adsorption occurs because the atoms at the surface of a solid experience an unbalanced normal force of attraction exerted by the interior atoms of the bulk solid. A balance of forces can be partially restored by forming bonds with gas molecules. Adsorption is spontaneous since the result is a decrease of the free energy of the solid-gas interface system [11].

2. Desorption

The rupture of the bond between a solid surface and adsorbed gas molecules resulting in the removal of those molecules from the surface is called desorption. It is the reversal of the process by which the bond was formed and requires the addition of energy to the solid-gas interface region [12]. This process may take place in equilibrium with adsorption or it may result from a relatively sudden perturbation. The latter case is referred to as induced desorption.

3. Metal Surface

The surface of a metal is the outer boundary which contains the bulk solid. An ideal metal solid-gas adsorption surface is a continuous geometric plane boundary between a free gas phase and a homogenous metallic conductor [13]. Real surfaces contain imperfections such as roughness, heterogeneity, and grain boundaries. These modify the ideal uniform adsorption potential as does the atomic periodicity of the lattice.

B. ADSORPTION PHENOMENA

1. Common Classification

There are two principal classifications of adsorption based on nature and strength of the bond formed. These two types of adsorpticn represent the extremes and there is no distinct division between them [14].

a. Physical Adsorption

Physical adsorption is the result of the intermolecular or van der Waals forces responsible for the condensation of a vapor to a liquid. The bonding energies are usually expressed in terms of heats of adsorption. These are on the order of 1.5-9.0 kcal/mole (0.06-0.36 eV/molecule). This is in the range of heats of condensation for common gases. Physical adsorption is rapid and reversible and the rate depends strongly on surface temperature [11].

b. Chemical Adsorption

Chemical adsorption involves the formation of a chemical bond , an exchange or sharing of electrons between the solid and the gas molecule. The bond energies are on the order of 20-40 kcal/mole (0.8-1.6 eV/molecule). This process is not necessarily rapid and may be very difficult to reverse [11].

2. Models

A complete empirical function for adsorption of a specific gas onto a given solid can be written as

$$v = f(p,T) \qquad (2-1)$$

where: v = gas volume adsorbed/ unit mass of solid
p = equilibrium gas pressure
T = surface temperature.

In practice, the quantity of interest for gas adsorbed on a solid surface is the surface area density (number of molecules adsorbed/ unit surface area of solid) or the fractional surface area covered by the adsorbed gas molecules [14]. For experimental purposes, it is desirable to express the adsorption function in terms of two variables with the third fixed. The most common form is the isotherm,

$$v = f_T(p). \qquad (2-2)$$

Detailed derivations and analysis of the various mathematical models used to describe adsorption can be found in Young and Crowell [11], Adamson [14], and Flood [15]. There are two major categories of adsorption models,

monolayer and multilayer. Chemical adsorption is in general restricted to a monolayer. Physical adsorption may occur in either a monolayer or in multilayers.

a. Monolayer Models

The majority of expressions of this type are based on the Langmuir isotherm [16]. The fundamental assumptions are

> "that the atoms (or molecules) of the gas are adsorbed as wholes on to definite points of attachment on the surface of the adsorber (adsorption sites), that each point of attachment can accomodate one and only one adsorbed atom, and that the energies of the states of any adsorbed atom are independent of the presence or absence of other adsorbed atoms on neighboring points of attachment [17]."

The Langmuir isotherm is

$$\theta = v/v_m = bp/(1+bp) \qquad (2\text{-}3)$$

where: θ = fraction of adsorption sites filled

b = constant [units 1/p] which depends on equilibrium adsorption-desorption rates

v_m = gas volume adsorbed per unit solid mass at infinite pressure (i.e. all sites filled).

Many refinements of the Langmuir isotherm have been derived which include such factors as surface mobility and lateral interactions of the adsorbed molecules and non-uniformities of the surface.

Another type of monolayer model draws an analogy between condensation of adsorbed films on solids and insoluble films formed on liquids. The isotherms for this type are derived from two dimensional equations of state. This type of model is very useful for determining surface areas of finely divided or porous solids.

b. Multilayer Models

There are three basic theoretical models used to describe multilayer adsorption and a multitude of permutations and refinements of each. The first is the Polanyi potential theory. It is historically the oldest and is still considered to be sound. This theory views the adsorbed layers of molecules as lying in a potential field which decreases with distance from the surface. The analogy is to the earth with its atmosphere decreasing in density outward from the surface. The equations developed describe the adsorption bond energy as a function of gas volumes contained between adsorbed layers and the surface [18].

The second basic model is the polarization theory proposed by deBoer and Zwikker. They assumed that the surface induced dipoles in the first layer of adsorbed molecules which in turn induced dipoles in the next layer and so on. The magnitude of the induced dipoles decreased exponentially with layer number. This is the least used of the basic models because the resulting isotherms expressed in terms of log(log p) versus v do not fit well with experimental observations [11].

The last and most common of the multilayer models is the BET isotherm (the term is derived from the first letters of the last names of the authors, Brunauer, Emmett, and Teller) [19]. This is a generalization of the Langmuir isotherm. The basic assumption is that the Langmuir isotherm applies to each layer, with each providing adsorption sites for the next outer layer. The first layer is assumed to have a certain heat of adsorption and all the rest have different but equal heats of adsorption which are equal to the heat of vaporization of the condensed adsorbed

gas. It is also assumed that vaporization and condensation can only occur at exposed surfaces. The individual isotherms are summed over all layers to yield the total adsorption isotherm. Refined versions of this model are frequently used to describe physical adsorption processes.

C. INDUCED DESORPTION METHODS

A concise review of desorption processes is given by Menzel [12]. The following is a brief summary of current desorption methods.

1. Thermal

Heating a solid-gas interface system imparts a Maxwellian distribution of energies to the particles in the adsorbed layer. When molecules in the higher energy portion of the distribution achieve energies greater than their adsorption bond energy, they leave the surface. This method is normally analyzed along lines similiar to chemical kinetics. The rate of desorption is determined as a function of temperature and concentration of particles per unit surface area. This is by far the oldest and most common method used to study desorption phenomena.

a. Flash Filament Technique

One of the most useful of the thermal desorption methods is the flash or flash filament technique. The procedure consists of recording pressure changes due to desorption when a thermally cleaned metal ribbon or wire exposed to a low pressure gas is rapidly heated. This

method can be used to determine desorption rates, surface coverages, or desorption activation energies [20]. The method was first used by Becker [21] and has been refined by Ehrlich [22] and Redhead [23]. The following derivation of an expression for desorption energy was based on these sources.

For a vacuum system in equilibrium at a certain temperature, the leak rate is given by

$$L = kSp_{eq} \tag{2-4}$$

where: L = leak rate (molecules/ unit time)

S = pumping speed (volume/ unit time)

p_{eq} = equilibrium pressure

k = constant = 3.27×10^{19} molecules/liter-Torr (value for N_2 at p=1Torr and T=295°K).

If the heating of the metal sample is fast, it can be assumed that no readsorption of gas onto the metal surface occurs during the heating. Then the number of molecules entering the free gas phase in the chamber per unit time can be related to the chamber pressure by

$$AN_d + L = kSp + kV(dp/dt) \tag{2-5}$$

where: A = surface area of the heated metal

N_d = desorption rate/ unit area

V = volume of the vacuum chamber.

Combining (2-4) and (2-5) yields an expression for the gas desorption rate in terms of the chamber pressure increase,

$$aN_d = dp^*/dt + p^*/t_c \tag{2-6}$$

where: $p^* = p - p_{eq}$

t_c = characterictic pumping time = V/S

$a = A/(kV)$.

By taking dp^*/dt equal to zero at the point of maximum pressure increase, which is also the point at which the desorption rate is a maximum, (2-6) becomes

$$(N_d)_{max} = p^*_{max}/(at_c) = (kS/A)p^*_{max} \qquad (2\text{-}7)$$

The desorption rate is usually expressed in chemical kinetic terms as a function of concentration of adsorbed gas particles and of surface temperature,

$$N_d = f(n_s, T) = -dn_s/dt = (n_s)^j u_j, \qquad (2\text{-}8)$$

where: n_s = surface coverage (molecules/ unit area)

T = surface temperature

u_j = reaction rate

j = desorption reaction order.

The reaction order defines the power law dependence of the rate of a desorption reaction on the surface coverage of adsorbed molecules. An experimentally measured kinematic reaction order is interpreted as an indication of the specific mechanism by which a chemical reaction takes place.

The desorption rate (2-8) is usually analyzed in terms of an Arrhenius equation of the form

$$N_d = (n_s)^j u^0_j \exp[-E_d/RT] \qquad (2\text{-}8a)$$

where: u_j^0 = rate constant independent of temperature

E_d = desorption bond energy

R = universal gas constant = 8314.1J/kmole°K.

The temperature dependence is assumed to be entirely contained in the exponential term. The concepts behind (2-8a) are

> "that the coverage term, $(n_s)^j$, is produced by the number of particles taking part in the critical step (desorption), the pre-exponential, u_j^0, is equal to the frequency of attempts of the system to move in the direction of the reaction, and the exponential term represents the relative number of these attempts having the necessary minimum energy [12]."

As initial approximations, a first order reaction (j=1), a rate constant equal to the lattice vibration frequency of metals at room temperature (u^0 of the order of 10^{13} sec^{-1}), and a monolayer coverage of adsorbed gas molecules ($n_s = 10^{15}$ molecules/cm^2) are usually assumed. If a further assumption that the time of the desorption rate maximum is coincident with the time of maximum surface temperature during the flash heating, (2-8a) can be written as

$$(N_d)_{max} = n_s u^0 \exp(-E_d/RT_{max}) \qquad (2\text{-}9)$$

or, by substituting for $(N_d)_{max}$ from (2-7), as

$$(kS/A)\, p^*_{max} = n_s u^0 \exp(-E_d/RT_{max}). \qquad (2\text{-}10)$$

Equation (2-10) can be solved for an approximate value of E_d,

$$E_d = -RT_{max} \ln[(p^*_{max})Sk/(An_s u^0)]. \qquad (2\text{-}11)$$

It must be emphasized that this is only a first approximation which required several assumptions and neglected such factors as end effects and adsorption-desorption from the walls of the chamber. However, as a macroscopic description of a sequence of unknown and complicated microscopic processes, it does offer a starting pcint for investigation. The above model is very similiar to the case of rapid surface heating of a target spot by laser radiation resulting in photon-induced thermal desorption.

2. Electron Impact

Electrons impacting with adsorbed particles in the ground state can cause electronic transitions to excited states or may result in ionization of the adsorbed atom or molecule. These excited particles may have sufficient energy to escape the potential well of the adsorption bond and leave the surface . For metal-gas interfaces, electron energies greater than 10 eV have been observed to cause electron impact desorption of ions and neutrals [12].

3. Photon-induced

Photons can cause desorption of gas from a metal surface by either direct excitation similiar to excitation by electron impact or by heating the metal causing desorption by thermal processes. The specific interaction will depend on the energy of the photons, the photon flux or light intensity, and the thermodynamic properties of the interface system under the influence of the incident photons. These processes will be discussed in detail in later sections. Laser induced desorption is a special case of this type of desorption.

4. Ion Impact

Ions impacting on the solid-gas interface can cause desorption by either direct transfer of energy to the adsorbed molecule or by inducing cascade collision chains within the solid which eventually knock off an adsorbed molecule from the surface. This process is very similiar to the sputtering of a substrate material. Desorption by impact of fast neutral molecules or neutrons occurs by the same processes as desorption by ion impact.

5. Field Emission

Under the influence of a very large electrostatic field (of the order of 10^8 V/cm concentrated in the region of the adsorbed layer which is a few angstroms thick), the rupture of the bond between an adsorbed gas molecule and a positive metal surface may occur by a transition from the ground state to the field deformed ionic state. This process is similiar to field ionization. The strong

electric field lowers the ionic potential towards the relatively unaffected ground state potential until the two are separated by an energy difference smaller than the thermal desorption energy. If sufficient energy from thermal motion is available, the gas molecule can make an adiabatic transition from the bound adsorbed state to the free ionic state [12].

III. PHOTON-INDUCED DESORPTION

As previously stated, photon-induced desorption of a gas from a solid surface can occur by two different processes. The first of these is direct excitation. In this process, usually termed photodesorption, incident photons excite adsorbed gas molecules to higher energy states from which they depart the surface with kinetic energy equal to the difference between the photon energy and the adsorption bond energy [24]. The second process is simply thermal desorption due to increased surface temperature of the solid caused by a transfer of incident photon energy to heat. The latter effect is always present for opaque solids and can be made negligible only for very low incident photon intensities [4].

A. PHOTODESORPTION

The existence of this process is the subject of some controversy. The reason for this is that it is difficult to eliminate phcton-induced thermal desorption when conducting experiments. However, there have been several reported observations of photodesorption [4-6, 10, 24-27]. So far, carbon monoxide is the only gas observed to have been photodesorbed and only photons with wavelengths in the visible and shorter regions of the spectrum have been observed to cause photodesorption [27].

The photodesorption process is similar to that for molecular dissociation of a diatomic molecule [24]. For

photons of a given quantum of energy, the desorption rate can be expressed as

$$N_d = \phi_i n_s \sigma \qquad (3\text{-}1)$$

where: N_d = number of molecules desorbed/ unit area and unit time

ϕ_i = incident photon flux

n_s = number of molecules adsorbed/ unit area

σ = photon-molecule interaction cross section area.

The quantum efficiency of the photodesorption process in terms of the number of molecules desorbed per incident photon is

$$\text{Eff.}_Q = n_s \sigma \qquad (3\text{-}2)$$

Observers are in general agreement regarding two facts. First, photodesorption is a very inefficient process for ultraviolet and visible wavelength photons. The efficiency decreases with increasing wavelength. This is reasonable since the more energetic short wavelength photons cause adsorbed molecules to be excited to higher energy states from which they can more easily leave the surface. Reported experimental quantum yields of photodesorbed gas molecules from metal surfaces are of the order of 10^{-7}-10^{-9} desorbed molecules/ incident photon [4-6]. Second, only a slight photon-induced surface temperature increase (estimated to be less than 20 - 50°C) can be permitted if detectable gas release due to thermal desorption is to be avoided during an experiment [4, 25]. This can only be achieved by using very low light intensities (of the order of microwatts/ square centimeter). Thus, there is a problem involved in observing photodesorption, i.e., the low efficiency of the process

requires a large incident photon flux to yield measurable results; but this in turn causes a greater temperature rise than is acceptable to eliminate thermal desorption [4]. For the case of induced desorption by infrared laser pulses, both the high intensity and long wavelengths involved would indicate that photon-induced thermal desorption is the predominant effect.

If a monolayer coverage of about 10^{15} molecules/cm^2 is assumed and substituted into (3-2), the result implies that the photodesorption cross section must be very small to cause such low reported efficiencies [6]. The reason for this is that not every incident photon will interact with a gas molecule adsorbed on a solid surface. Some photons will be reflected and others will contribute to heating the surface. In addition, once photoexcitation of an adsorbed gas molecule has occurred, desorption is not the only process which can follow. The energy of excitation can be dissipated into the solid lattice as well as causing disruption of the adsorption bond. It has been estimated that this de-excitation process is very fast on metal surfaces (of the order of 10^{-15} sec) [26, 28]. Thus, the probability of photodesorption is very small. This accounts for the overall low efficiency of the process.

B. PHOTON-INDUCED THERMAL DESORPTION

If photon energy striking a metal target is absorbed and causes an increase in surface temperature, thermal desorption will take place. In order to relate this process to existing thermal desorption methods, an expression for the surface temperature increase as a function of incident

photon intensity must be developed. The following derivation has been adapted from Bechtel [29], Schriempf [30], and Fuhs [31]. Since photon-induced desorption by infrared laser pulses was the topic of study, specific assumptions will be made to apply the general development to that case.

1. Coupling of Photon Energy with Metal Targets

The amount of incident photon radiation absorbed by a solid, opaque, metal target is

$$I_a = (1-R) I_i \cos\alpha \qquad (3-3)$$

where: I_a = intensity absorbed by the target

I_i = intensity incident on target

R = reflectivity of the target surface

α = angle of incidence with surface.

Experimental evidence has shown that a Drude-Lorentz free electron model for metals is justified for interactions with infrared wavelength photons [30]. With this model, electromagnetic radiation interacts only with free electrons in a metal. These electrons are raised to higher energy states upon absorption of photons and transfer this energy to other electrons and to lattice ions by collisions. Heating is the result of these collisions. The mean free time between collisions in a metallic conductor is of the order of 10^{-13} seconds. During light pulses of the order of a nanosecond, electrons in a metal target will make many collisions. The photon energy is therefore assumed to be transformed instantaneously to heat at the point of absorption [32].

2. The Heat Conduction Equation

The classical thermodynamic heat conduction equation is given by

$$\nabla \cdot \bar{J}(\bar{r},t) + \rho C \partial T(\bar{r},t)/\partial t = A(\bar{r},t) \qquad (3\text{-}4)$$

where: $\bar{J}$ = heat flux

ρ = density of metal target

C = specific heat of metal target

T = temperature

A = net energy/ unit volume and unit time generated by absorbed photons.

The relation between heat flux and temperature is given by Fourier's Law,

$$\bar{J}(\bar{r},t) = -\bar{K}\bar{\nabla}T(\bar{r},t) \qquad (3\text{-}5)$$

where: $\bar{K}$ = thermal conductivity tensor.

Substituting (3-5) into (3-4) yields

$$\nabla^2 T(\bar{r},t) - (\rho C/\bar{K})\partial T(\bar{r},t)/\partial t = -A(\bar{r},t)/\bar{K} \qquad (3\text{-}6)$$

In order to obtain a solution to (3-6), $A(\bar{r},t)$ and the physical properties of the target metal must be known and the boundary conditions for the specific case of interest must be specified. For real world situations, these quantities may be very complicated and lead to impossibly complex differential equations. Because of this several simplifying assumptions are made:

a) No phase change from solid to liquid or vapor occurs. This is justified for nancsecond laser pulses with intensities $\leq 10^8$ W/cm^2.

b) Material properties are temperature independent.

c) The metal is uniform and isotropic. This implies that $\bar{K}$ becomes a scalar constant.

d) The target is taken as a semi-infinite slab with surface normal parallel to the z axis [Fig. 1].

e) Only times such that the diffusion length of heat in the radial direction is small compared to the radius of the incident beam are considered.

f) There is an exponential attenuation of the absorbed photon radiation with distance into the target. This distance is the skin depth, d'.

g) The photon intensity is azimuthally symmetric.

With the above assumptions, (3-6) reduces to

$$\partial^2 T(z,t)/\partial z^2 - (\rho C/K)\partial T(z,t)/\partial t = -(1/K)(1/d')\exp(-z/d')I_a \qquad (3-7)$$

3. Surface Generation of Heat

Since the skin depth for metals is very small (of the order of 100 angstrom), the heat due to absorbed photons can be considered to be generated at the surface. For this situation, (3-7) can be reduced to a homogenous equation

$$\partial^2 T(z,t)/\partial z^2 - (\rho C/K)\partial T(z,t)/\partial t = 0 \qquad (3-8)$$

with boundary condition

$$-K(\partial T/\partial z)_{z=0} = I_a . \qquad (3-9)$$

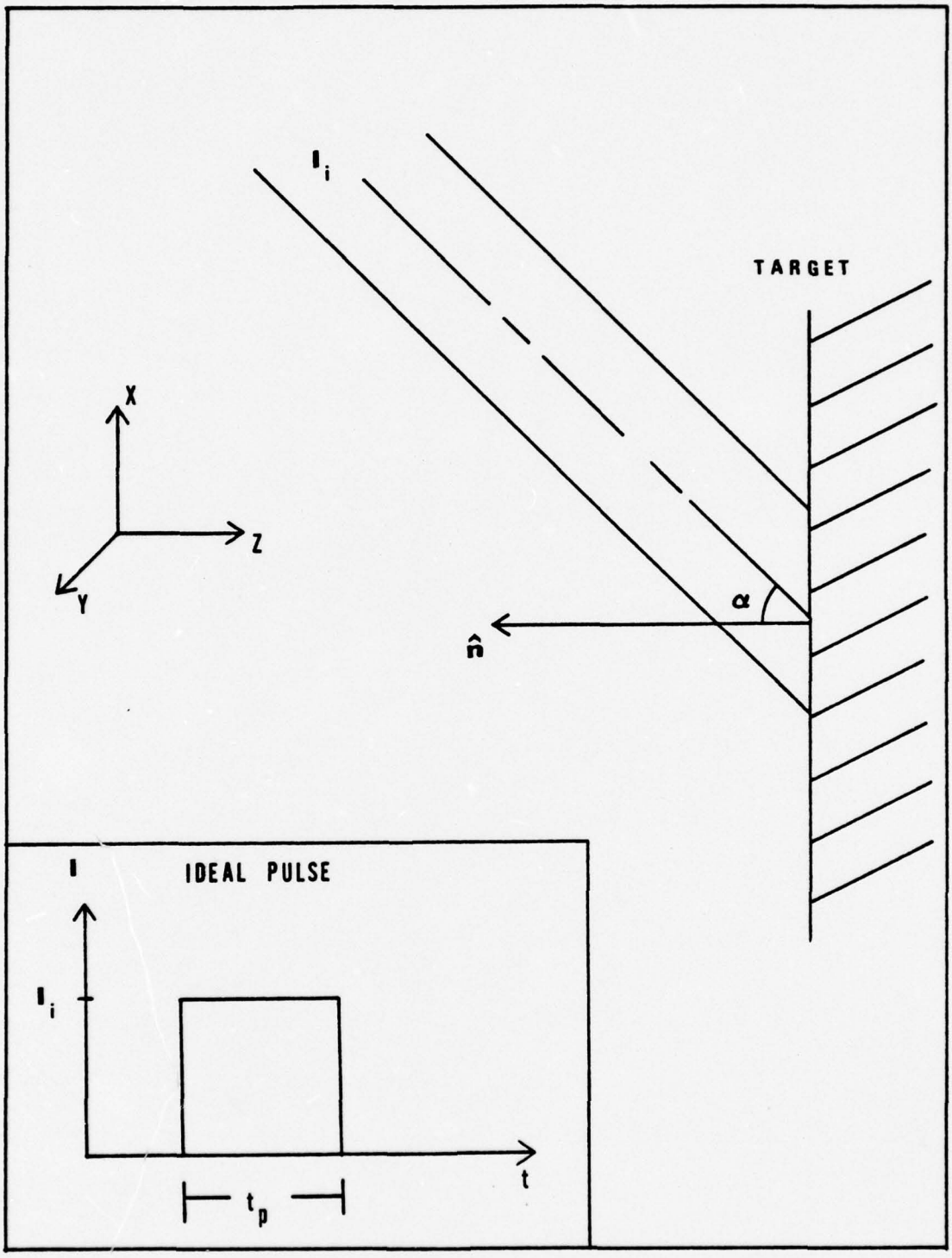

Figure 1 - SCHEMATIC DIAGRAM OF TARGET AND INCIDENT LASER PULSE

4. Heating of Solids by Laser Pulse

If the incident photon radiation is produced by a Q-switched laser, I_i may be approximated by an ideal pulse with constant uniform intensity of duration t_p (Fig. 1). The solutions of (3-8) for this case may then be obtained. As given in Ref. 29 they are:

$$\Delta T(0,t)\begin{cases} = 0 \quad , t<0 \\ = (2/K)\,(Kt/\rho C\pi)^{1/2} I_a \quad , 0\le t\le t_p \\ = (2/K)\,(K/\rho C\pi)^{1/2}\,[(t)^{1/2}-(t-t_p)^{1/2}]I_a \quad , t>t_p . \end{cases} \tag{3-10}$$

A plot of surface temperature change of a stainless steel target versus time calculated from (3-10) is shown in Fig. 2. The assumed values for the bulk thermodynamic properties are the average values between room temperature and the melting point for 304 stainless steel given in Ref. 33. From Fig. 2, it can be seen that the maximum surface temperature increase occurs at time t_p.

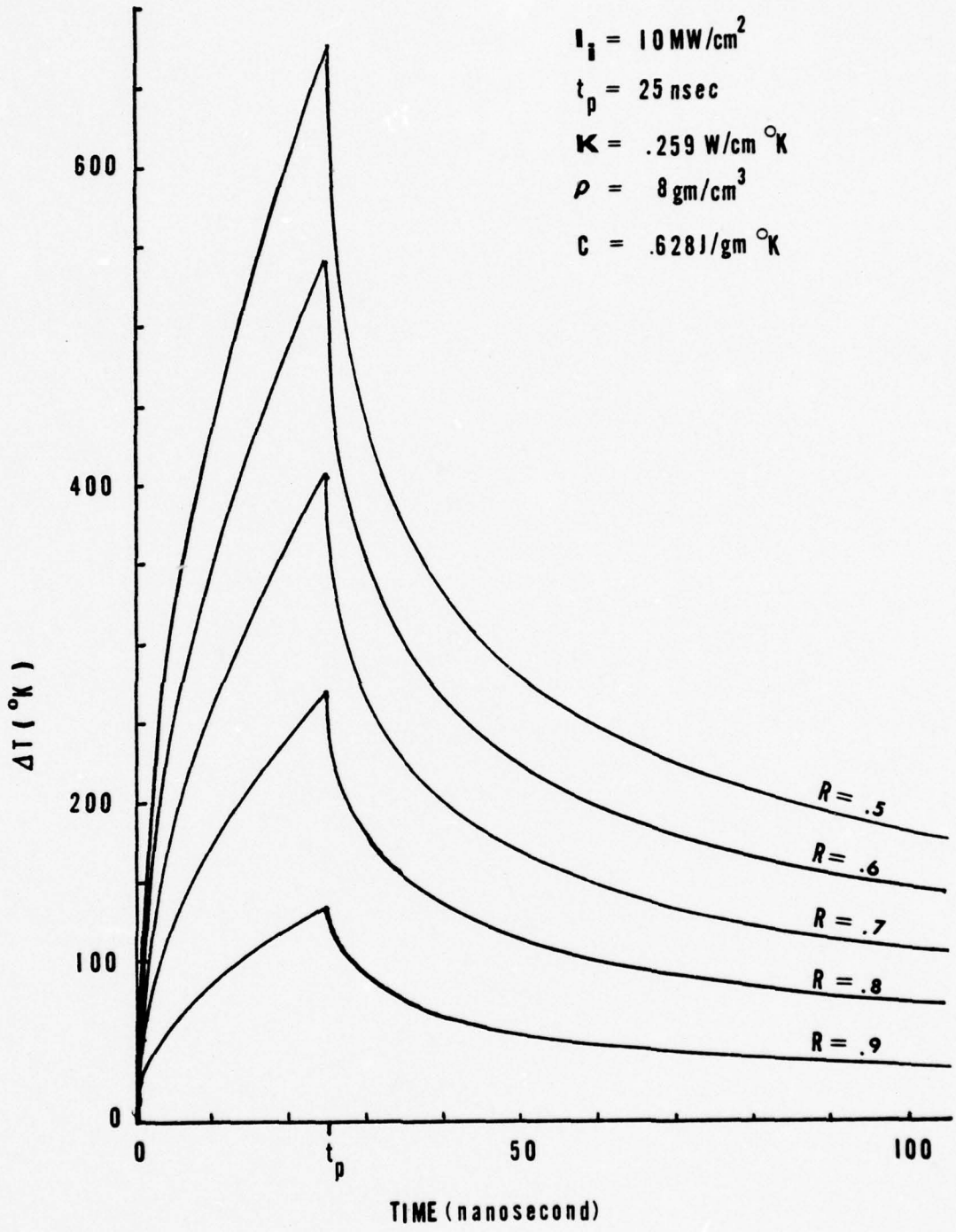

Figure 2 - LASER INDUCED SURFACE TEMPERATURE INCREASE

IV. EXPERIMENT

A. EQUIPMENT ARRANGEMENT

A schematic of the experimental apparatus is shown in Fig. 3.

1. Laser System

A Q-switched neodymium-doped glass laser was the source of 1.06 micrometer wavelength photons. The laser had a 25 nanosecond (FWHM) pulse width. The unfocused beam had a cross sectional area on target of $4.1 \pm .2$ cm^2. The physical geometry of the equipment was such that the incident beam struck the target at an angle of 30° to the surface normal. A detailed description of the laser system is given in Appendix A.

2. Test Chamber

The main test chamber was an unbaked aluminium vessel with a $12.9 \pm .3$ liter volume. Various ports allowed mounting of valves, gauges, a mass spectrometer, feedthroughs, and observation windows. The chamber was evacuated tc pressures of the order of 4×10^{-7} Torr by an oil

diffusion pump through a liquid nitrogen cold trap. A system of valves and piping allowed for isolation of the chamber from the pumps. A gas bleed system allowed flooding of the chamber with a test gas at different pressures. A complete description of all of the chamber components is contained in Appendix B.

3. Target

The metal targets used were disks 5.0±.1 cm in diameter and 0.6±.05 cm thick. The disks were machined from 304 stainless steel stock. A hole was drilled and threaded through the center of each disk for mounting on a rotating feedthrough inside the test chamber. Some targets were used as received with only degreasing. Others were polished with a series of ever finer grits down to a 0.05 micrometer Al_2O_3 slurry and then ultrasonically cleaned.

The polished targets were weighed prior to and after laser firings. The surface reflectivity of the polished targets was determined using incident radiation from a CW Nd:YAG laser (wavelength 1.06 micrometer). The power of the incident beam was measured with a disk calorimeter and then the target and calorimeter arranged to measure the power reflected from the surface. The reflectivity was then calculated as

$$R = P_r/P_i . \qquad (4-1)$$

The reflectivity of the polished target surfaces was approximately 67%. The reflectivity of the rough targets was not measured.

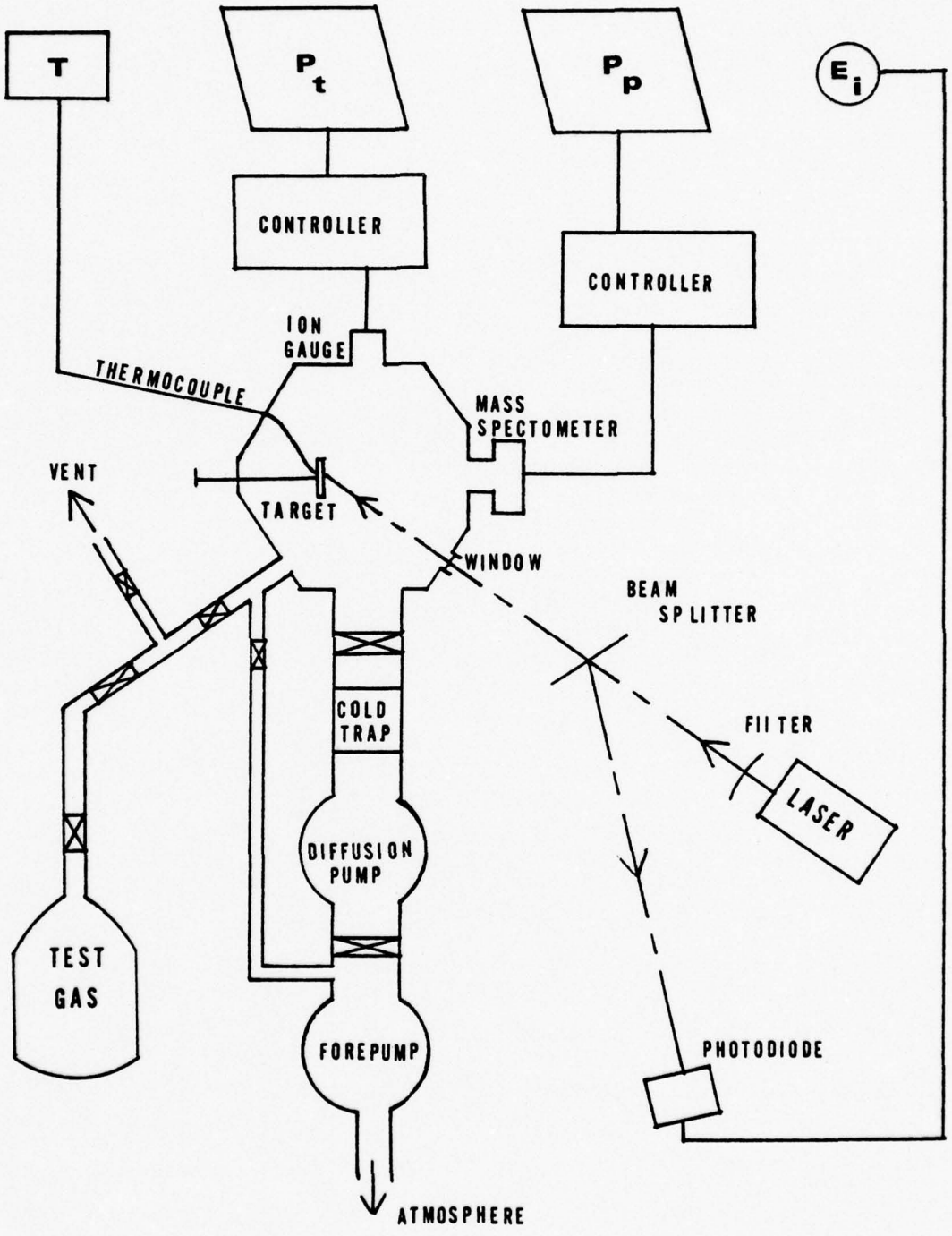

Figure 3 - SCHEMATIC OF EXPERIMENTAL ARRANGEMENT

B. PROCEDURE

A target, after cleaning or degreasing, was mounted in the chamber. The entire system was pumped down to the diffusion pump base pressure and left under vacuum at room temperature for at least 24 hours prior to taking data. After this period of time, all gauges, meters, and recorders were setup, energized and calibrated.

A background gas pressure mass spectrometer sweep for 1-10 AMU and 10-70 AMU mass ranges was made prior to laser firings. From this background, the mass spectrometer settings were selected to read partial pressure of one specific species. Data were taken for four different species: H_2O^+, CO_2^+, N_2^+/CO^+ (the instrument could not distinguish between these two), and H_2^+. These were chosen because their partial pressure peaks were easily identified from the spectrum sweep and because each had been reported to be present on stainless steel surfaces at room temperature [1]. For each gas, a series of laser pulses at one energy level were then fired at the same spot on the target.

For each laser pulse, the energy of the pulse, the total pressure increase inside the chamber, the partial pressure increase of the selected species and the ambient temperature of the target (measured at the rear surface) were recorded. The target was then rotated and another series of pulses at a different energy level were fired at the new target spot. A total of three target spots could be accomodated without

overlap on one face of the disks. Therefore, three laser output pulse total energy levels were used: 2.0J, 1.5J, and 1.0J.

The entire sequence above was then repeated. The difference was that prior to each laser pulse the chamber was flooded to about 4×10^{-5} Torr with the gas for which partial pressure was being recorded. The gases used for the data sequences with flooding were CO_2, N_2, and H_2. At the end of each data sequence, a final background gas pressure sweep was made to check for possible changes during the course of laser firing.

V. RESULTS

A. TEST DATA

1. Target Reflectivity

The observed changes in target reflectivity due to laser radiation damage were small (of the order of 0-3%). The reflectivity of the polished target surfaces irradiated by the laser pulses varied from 67% (no change from the original reflectivity) for areas subjected to a series of 1.0J pulses to 64% for those struck by a 2.0J pulse series.

There were no provisions for monitoring any changes of surface reflectivity during a laser pulse. Reflectivity measurements have been reported which used integrating spheres to collect radiation reflected from metal surfaces irradiated by Q-switched Nd-glass lasers. The results obtained indicated that, for incident pulse intensities below 100 MW/cm^2, the average reflectivity coefficients remained very near their undisturbed values for the duration of the pulse [32].

It was noted also that there was slight, irregular marring and discoloration of the target surfaces at spots irradiated by pulses with energies greater than about 1.5J. This was due to the nonuniform intensity distribution of the

laser beam and also due to nonuniform reflectivity caused by individual surface defects. These effects have been previously observed [2,7]. However, there were no major damage spots nor was pitting observed. A check of target weight revealed no detectable loss of material (less than 0.01 grams) from the targets.

2. Pressure Changes due to Desorption

The most noticeable effect was the "cleaning effect" of the first three or four pulses of a series. The fact of the first few laser pulses of a series causing a much higher pressure increase within the test chamber than the pressure increase due to later pulses has been previously reported [7,9]. The first few laser pulses striking a target surface caused the removal of polishing compound residues, desorption of impurities adsorbed when the target was exposed to air, and the breakdown of vacuum pump oils which adhered to the surface after mounting the target inside the chamber. Hence the term "cleaning" of the surface. Fig. 4 shows a typical plot of the maximum total pressure increase as a function of pulse number for three different energy levels. This effect was observed for both total and partial pressure readings, for rough and smooth target surfaces, and for laser pulse series with and without a test gas flood of the chamber prior to each laser pulse.

A second feature of the observed pressure changes due to laser induced desorption is also shown in Fig. 4. That feature was the relatively constant maximum pressure increase due to the later laser pulses of a series. Both total and partial pressure readings exhibited this feature. In general, the magnitude of the constant maximum pressure increase per laser pulse grew as the total pulse energy increased.

For the rough targets, both the total pressure and the partial pressure changes per laser pulse were larger than the readings observed for the polished targets. This was true for laser pulse series with and without gas flood. There were two possible reasons for this. First, the rough targets had greater surface areas than did the polished targets. Thus, they provided a larger number of adsorption sites for gas molecules. Second, the reflectivity of the rough target surfaces was less than that of the polished surfaces. More incident photons were therefore absorbed which produced a greater photon-induced thermal desorption effect.

The flooding of the chamber with a test gas prior to each laser pulse did not cause any measurable difference in the maximum total pressure increase per laser pulse compared to similiar readings taken when a gas flood was not used between pulses. However, the maximum partial pressure increase per laser pulse was larger when gas flooding was used than the partial pressure change when flooding was not employed. Flooding the chamber with a test gas and then pumping the system back down to base pressure would not have greatly affected the total amount of all gases which could have been adsorbed onto the surface of the metal. However, flooding with a test gas would have increased its concentration inside the chamber and thus enhanced the adsorption of that gas onto the surface. Fig. 5 shows the partial pressure increase of hydrogen caused by 1.5J laser pulses as a function of pulse number for smooth and for rough targets both with and without hydrogen gas flood.

The observed maximum partial pressure increase per laser pulse was approximately one order of magnitude less than the maximum total pressure increase measured for the same pulse series. There were possibly small contributions to this difference from two different gauge sensitivities

and from independent meter calibrations. However, the most probable causes of the difference in measured pressures were that the test chamber was not a perfectly air tight vessel and that water vapor could not be removed from the chamber by a bake out procedure. The test gas for which partial pressure was being measured was in competition with air and water vapor for adsorption sites on the target surface. Therefore, the total amount of gas desorbed from the target per laser pulse consisted of a mixture of all gases inside the chamber but the mass spectrometer recorded the partial pressure of only one species at a time.

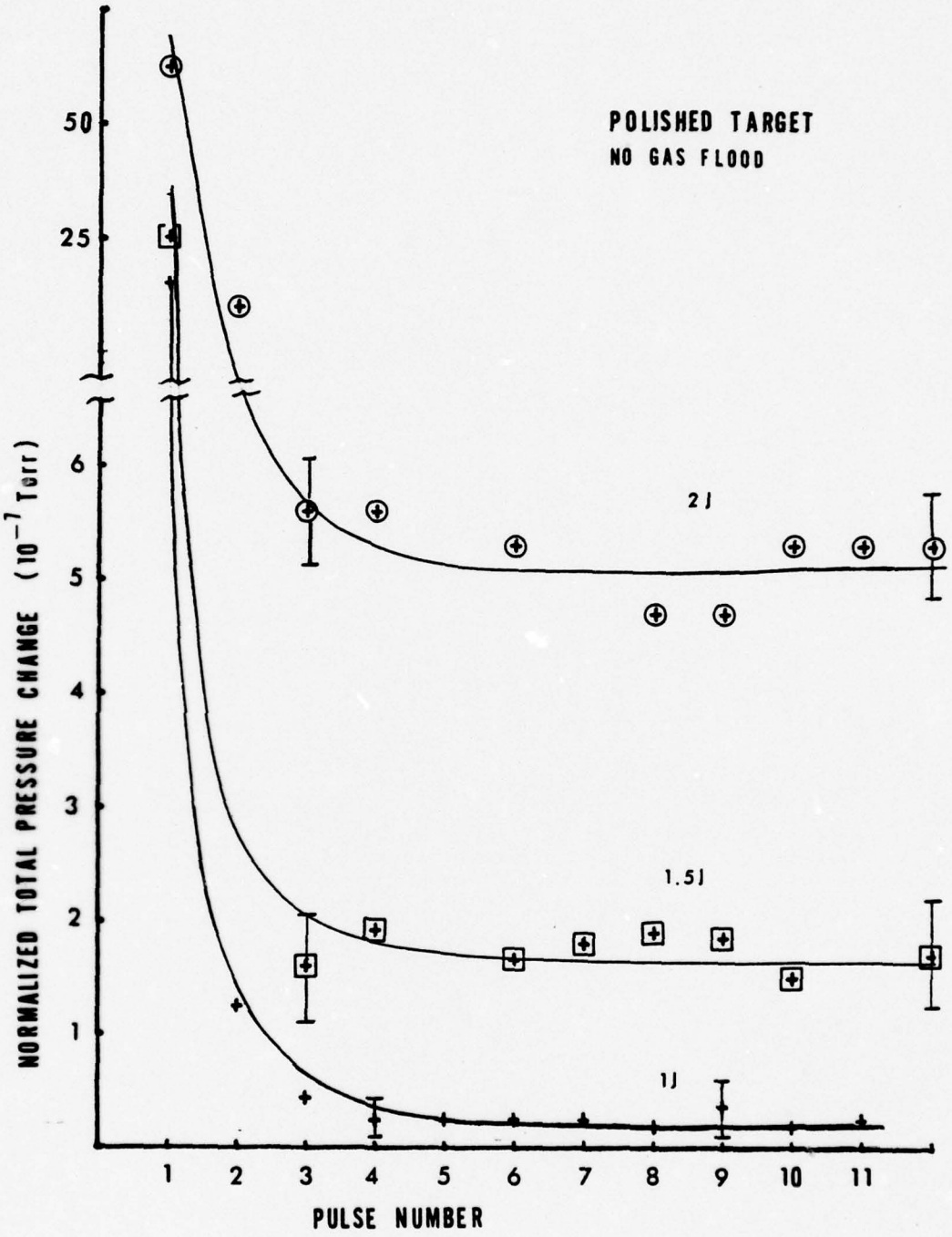

Figure 4 - CLEANING EFFECT

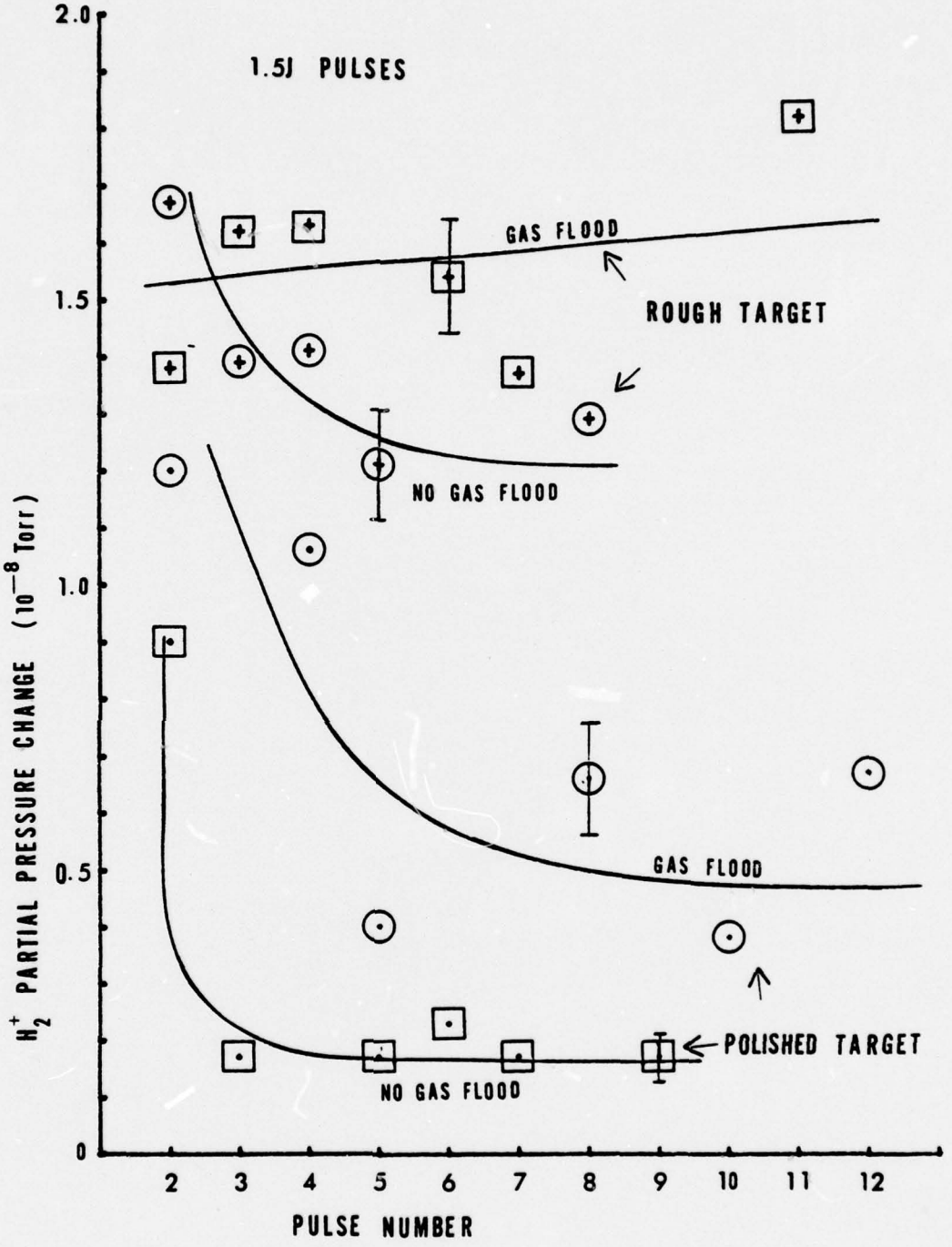

Figure 5 - EFFECT OF GAS FLOOD AND SURFACE ROUGHNESS

B. ANALYSIS OF DATA

1. Desorption Mechanism

As discussed in Sections II and III, if the laser induced desorption of gas from the target surfaces were due to direct excitation, the number of desorbed molecules (and hence the pressure increase) should show a linearly proportional rise with increasing pulse energy (directly related to total number of incident photons). On the other hand, the photon-induced thermal desorption effect should cause a maximum pressure increase per laser pulse which would vary exponentially with surface temperature (proportional to pulse energy). It was further stated that the photon-induced thermal effect was expected to be the predominant effect for the case of laser induced desorption because of the high incident photon intensities involved. Fig. 6 shows a plot of average partial pressure peak increase after the cleaning effect abated as a function of incident laser energy for H_2^+, CO_2^+, and N_2^+/CO^+. The curves show a decidedly nonlinear rise of peak pressure increase with laser pulse energy for H_2^+ and CO_2^+. These curves suggest that the primary desorption mechanism for laser induced desorption from metal surfaces is indeed photon-induced thermal desorption.

2. N_2^+/CO^+ Anomaly

The measured partial pressure increase per laser pulse of N_2^+/CO^+ shown in Fig. 6 remained nearly constant with increasing pulse energy. This was not in agreement with the results obtained for H_2^+ and CO_2^+. This anomaly has at its roots the inability of the mass spectrometer to differentiate between two species with the same charge to mass ratio (such as N_2^+ and CO^+). Lange has previously commented on the difficulties that can arise in interpreting the data obtained when this instrument limitation exists [4].

An explanation for this anomaly can be given based on this instrument limitation, the procedure used during the chamber flooding process, and the vacuum limits of the chamber and pump system. CO appears to be readily adsorbed and desorbed from metal surfaces. This can be seen from the photodesorption experiments described in Section III. In desorption experiments involving mixtures of N_2 and CO, Lange observed a thermal desorption ratio for CO to N_2 of eight to one [24]. After each laser pulse, the gas-metal surface interface system tended to reestablish equilibrium. If all desorbed molecules were not pumped out of the chamber (and it was not expected that they would be, given the slow pumping speed compared with the rapid heating and cooling of the surface as a result of an incident laser pulse), the

remaining CO would tend to readsorb more quickly than other gases present in the system and occupy more of the available adsorption sites. Some CO was also probably formed under the influence of laser radiation by dissociation of carbon dioxide and by reactions between oxygen which leaked into the chamber and the carbon in the stainless steel. These sources would tend to replenish the CO removed by the pump.

Given these factors, coupled with the fact that it took approximately one minute to establish a flow of test gas into the chamber from the gas bleed system after each laser pulse, the CO would have had ample time to establish itself on the surface. Therefore, although an N_2 gas flood was used when measurements were taken, the mass spectrometer partial pressure reading for N_2^+/CO^+ desorption pressure increase would have been dominated by CO. A relatively constant signal with increasing pulse energy would then be registered assuming even the lowest energy pulse was sufficient to desorb all of the CO on the surface.

3. Adsorption Competition and Equilibrium

Macroscopically, the adsorption process can be described as an equilibrium process for a given pressure and temperature. Microscopically, individual molecules are constantly being adsorbed onto, desorbed from, and transferred laterally across the surface of a metal target. These processes are quite rapid. The time to establish a certain gas adsorption surface coverage on a metal can be calculated by

$$t_n = n_s/\beta\mu = n_s/[\beta(N_a p)/(2\pi RMT)^{1/2}] \qquad (5\text{-}1)$$

where: t_n = time to establish a given coverage

n_s = surface coverage (molecules/ unit area)

β = probability that impinging molecule sticks

μ = kinetic gas theory wall bombardment rate (molecules/ unit area and unit time)

N_a = Avagadro's Number = 6.0228×10^{23} molecules/mole

M = molecular weight of gas

R = universal gas constant.

Using (5-1) to calculate the minimum times to establish a monolayer coverage of air molecules at room temperature for pressures between 10^{-5} and 10^{-7} Torr with an assumed sticking probability of one, the required times are of the order of 0.1 to 10 seconds. Based on this and the fact that there was a five minute minimum duty cycle between laser pulses (ten minutes between pulses if the chamber was flooded with a test gas prior to each pulse), there should have been ample time for the gases inside the chamber (both test gases and air and water vapor) to establish a monolayer of adsorbed gas on the target surface prior to each pulse. This acccunts for the relatively constant pressure increase per pulse after the cleaning effect ceased.

4. Energy of Desorption

Equation (2-11) gives a first order approximation of the energy required to thermally desorb a gas from a metal surface as a function of surface temperature and chamber pressure increase. The maximum temperature of a stainless steel surface subjected to incident laser pulses of a given

intensity can be calculated by

$$T_{max} = T_a + \Delta T_{max} \qquad (5\text{-}2)$$

where: T_a = average ambient temperature

ΔT_{max} = maximum temperature increase from (3-10).

Using T_{max} from (5-2) and measured p^*_{max} for a range of incident pulse intensities, the desorption energy of a gas from stainless steel can be obtained from (2-11). This equation can be rewritten in the form

$$\underbrace{\ln(p^*_{max})}_{y} = \underbrace{(-E_d)}_{m}\underbrace{(1/RT_{max})}_{x} - \underbrace{\ln[Sk/(An_s u^0)]}_{b} \qquad (5\text{-}3).$$

The desorption energy is then the slope of (5-3).

The constant term can be evaluated for a monolayer coverage ($n_s = 10^{15}$ molecules/cm^2) and a reaction rate equal to metal lattice vibration frequency ($u^0 = 10^{13}$ sec^{-1}) assumptions as

$$-\ln[Sk/(An_s u^0)] = 14.897 \qquad (5\text{-}4)$$

where: S = pumping speed = 425 liter/sec

A = target spot area = 4.1 cm^2.

This value can be compared with experimental "intercept" values obtained from (5-3) as a check on the appropriateness of the combined assumptions.

Fig. 7 shows a plot of (5-3) for maximum partial pressure increases of H_2^+, CO_2^+, after abatement of the cleaning effect at incident total pulse energies of 1J, 1.5J, and 2J with a test gas flood prior to each pulse. The desorption energy of hydrogen was found to be 8.5 kcal/mole (.37 eV/molecule) and the desorption energy of carbon dioxide was determined to be 14.7 kcal/mole (.64 eV/molecule). The intercepts of the plots were 14.5 for hydrogen and 14.1 for carbon dioxide. These correspond closely to the estimated value from (5-4). This correlation for the constants does not confirm the validity of any individual assumption but merely indicates the macroscopic adequacy of the combined assumptions.

The experimentally determined desorption energies for H_2 and CO_2 are lower than reported heats of adsorption for these species on clean surfaces of pure iron: 9-32kcal/mole for H_2 and approximately 60kcal/mole for CO_2 [14,15]. However, stainless steel is not a pure substance but an amalgam of various elements. Therefore, close agreement of desorption energy values with pure metal values was not expected. Oxides which are known to be present on stainless steel surfaces would also change desorption energies from those observed for pure substances [4].

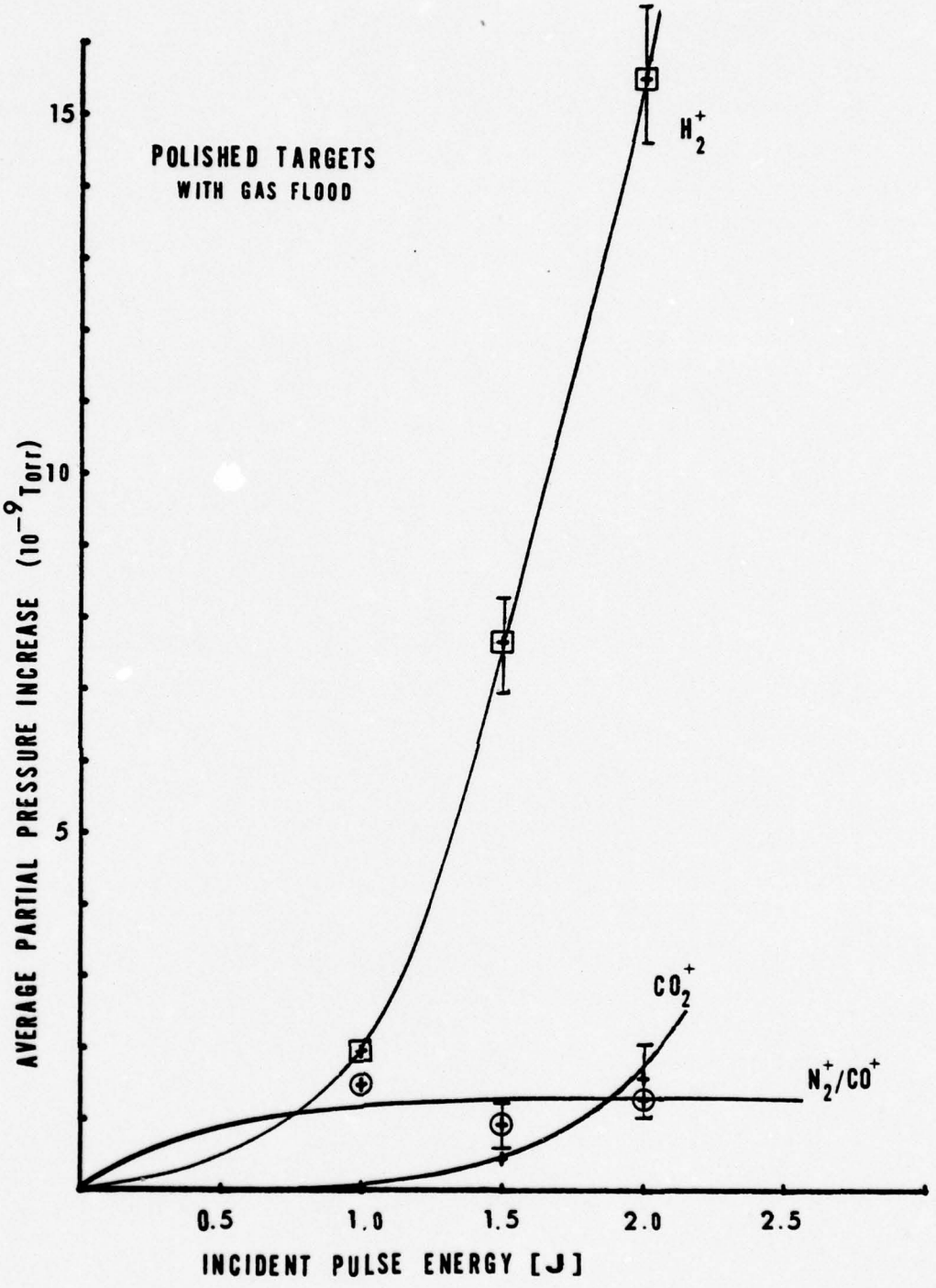

Figure 6 - PEAK PARTIAL PRESSURE INCREASE VERSUS ENERGY

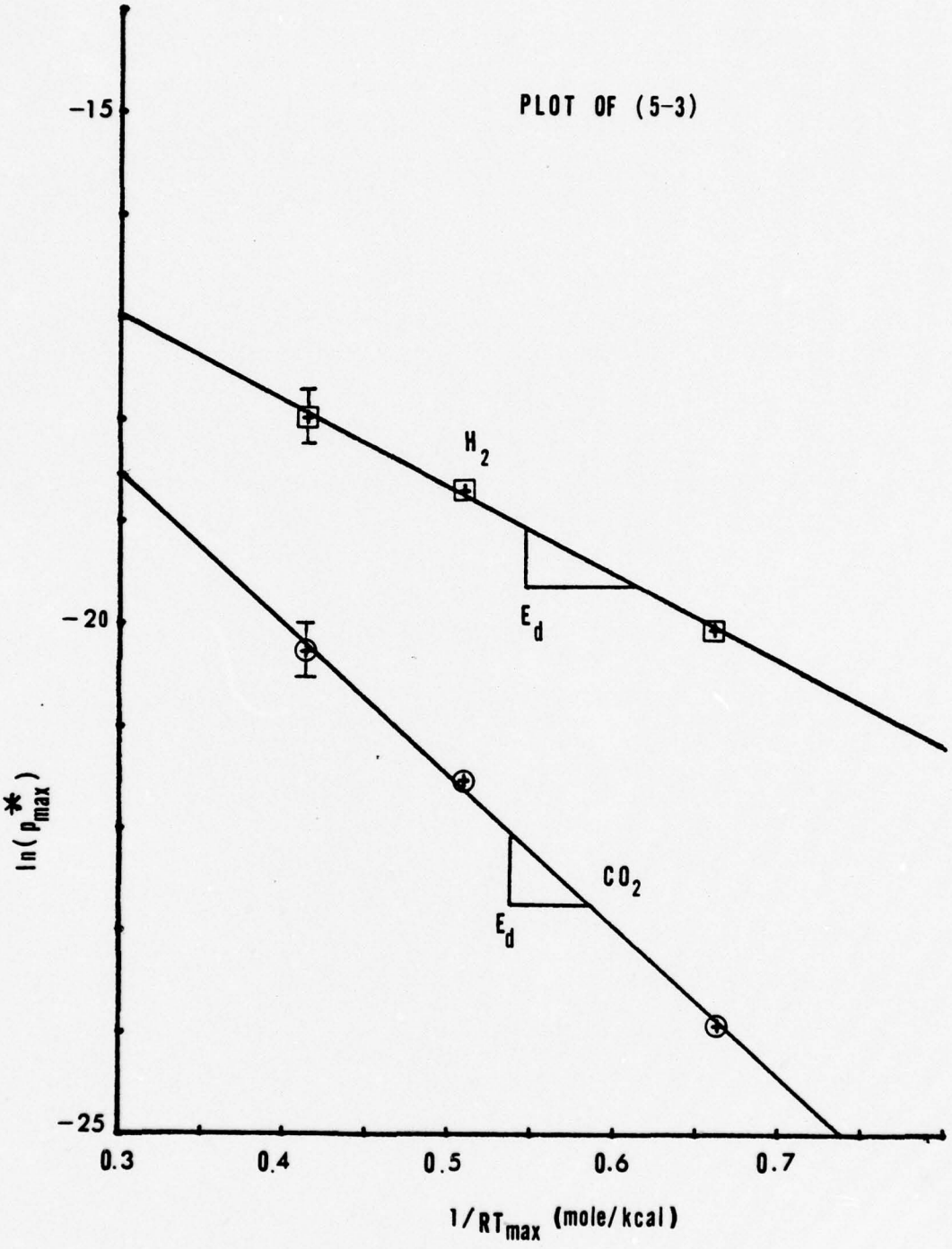

Figure 7 - DESORPTION ENERGY

VI. DISCUSSION

A. PROBLEMS AND RECOMMENDATIONS

There were three major problems encountered during the course of this experiment. The first was the inability of the mass spectrometer to differentiate between species with the same charge to mass ratios. This problem and the resultant anomaly have already been discussed.

The second difficulty encountered was in the control of laser pulse energy. The cross sectional energy distribution within the beam was not uniform and there was no way to alter this fact. The result was the minor surface damage noted for the hot spots of the higher energy pulses. In addition, the laser output could only be controlled to within about ±.3J of the desired energy. This required the pressure increases plotted in all figures to be normalized for the indicated pulse energy. This problem could be alleviated to some extent by including a spatial filter in the laser output path.

The final major problem was the vacuum limitation of the chamber and pumping system. The air leaks, pumping capabilities, and gauge sensitivity ranges limited the precision of the total pressure readings to an order of 10^{-6} Torr and the partial pressure readings to an order of

10^{-9} Torr. The air leaks also admitted contamination constantly into the chamber which resulted in the competition with the test gas for adsorption sites on the target surface. Considering the precision limits and the experimental conditions, the estimated uncertainties in the pressure readings were of the order of 10-15%.

B. CONCLUSIONS

The initial conclusion that can be drawn from the test results is that laser induced desorption of a gas from a stainless steel surface is predominantly a thermal effect. In addition, the results of this experiment indicate that laser induced desorption is a feasible tool to use in determining desorption energies for gases adsorbed onto metallic surfaces. To really test this as a reliable method, a greater range of incident laser intensities should be used. However, if surface damage is to be avoided, there is an upper limit to the allowed energy. To a degree, the concept of cleaning metal surfaces inside a vacuum chamber was also demonstrated. However, the latter use is accompanied by slight damage to the surface which may be unacceptable for many uses.

The target metal, stainless steel, and the gases used for this experiment were selected for convenience. Correlation with reported desorption results was small because these substances have not been widely used as gas-metal adsorption pairs. Further investigation of this phenomenon should use other more common experimental pairs to obtain correlations.

Several assumptions were made in developing the models used to find desorption energies. Among these were: constant values of reflectivity, uniform distribution of laser energy within the beam, ideal "top hat" pulse shapes, and ideal plane surfaces. None of the above was in fact true, although they are reasonable approximations.

The reflectivity of the target surfaces could not be measured during the time of the laser pulse irradiation. The functional dependence of the reflectivity on the surface temperature and its corresponding affect on the temperature change expression developed in (3-10) could not be assessed. The degree to which the actual reflectivity varied from the assumed constant value could change the calculated desorption energies significantly.

The ideal surface and pulse shapes and uniform distributions were assumed mainly for mathematical convenience. Calculations similiar to (3-10) have been worked out for Gaussian shaped pulses, but these add considerable complexity and are still only approximations [29]. Again, the results obtained were macroscopic descriptions of complex and varied microscopic processes.

APPENDIX A

THE LASER SYSTEM

The laser used was the two stage KORAD K-1500 Q-switched odymium-doped glass laser [34]. A general explanation of glass laser physics is given by Maiman [35]. The laser stallation at the Naval Postgraduate School Laser-Plasma boratory is detailed by Davis [36]. A block diagram of basic laser system components is given in Fig. 8.

The laser output energy was roughly controlled by tying the voltages applied to the oscillator and amplifier ashlamps. The energy range of the laser output was 5-15J. The pulse width was 25 nanosecond (FWHM). This s controlled by a Pockels cell Q-switching device mounted tween the oscillator and the rear reflector. The focused laser beam had an ellipical cross section. Finer ntrol of the output was obtained by mounting neutral nsity filters and/or lenses immediately after the plifier stage. For the experiments reported here, only lters were used.

Each filtered laser pulse passed through a thin pane of ass which acted as a beam splitter. The beam splitter flected a small portion of the output pulse onto a gnesium oxide block which in turn reflected it onto a otodiode detector. The detector output signal was fed to ektronix 564B storage oscilloscope. This detector signal l been correlated to total pulse energy measured by a lorimeter over a range from 0-15J.

Laser rod cooling was provided by a chilled water recirculating system. The parts of this system were a small refrigerator, a water pump, a water filter, two thermometers, a thermostatic temperature control and a reservoir of deionized water. The water was maintained at 20°C and a minimum cycle time between laser pulses of five minutes was allowed to insure adequate cooling of the rods.

Several power devices were associated with the laser system. A 10 kilovolt maximum variable charged capacitor provided power to the amplifier flashlamp. A 5 kilovolt maximum variable charged capacitor provided power to the oscillator. An HV-1565 2000 volt DC power supply energized the photodiode detector. An integral adjustable shutter control powered the Pockels cell device.

A CW He-Ne laser provided visual alignment and target position reference for the laser system. For safety, a red warning light outside the lab was energized during laser firings. A warning bell also sounded whenever the laser power supplies were charging. A detailed laser operating procedure and general safety precautions are given by Callahan [37].

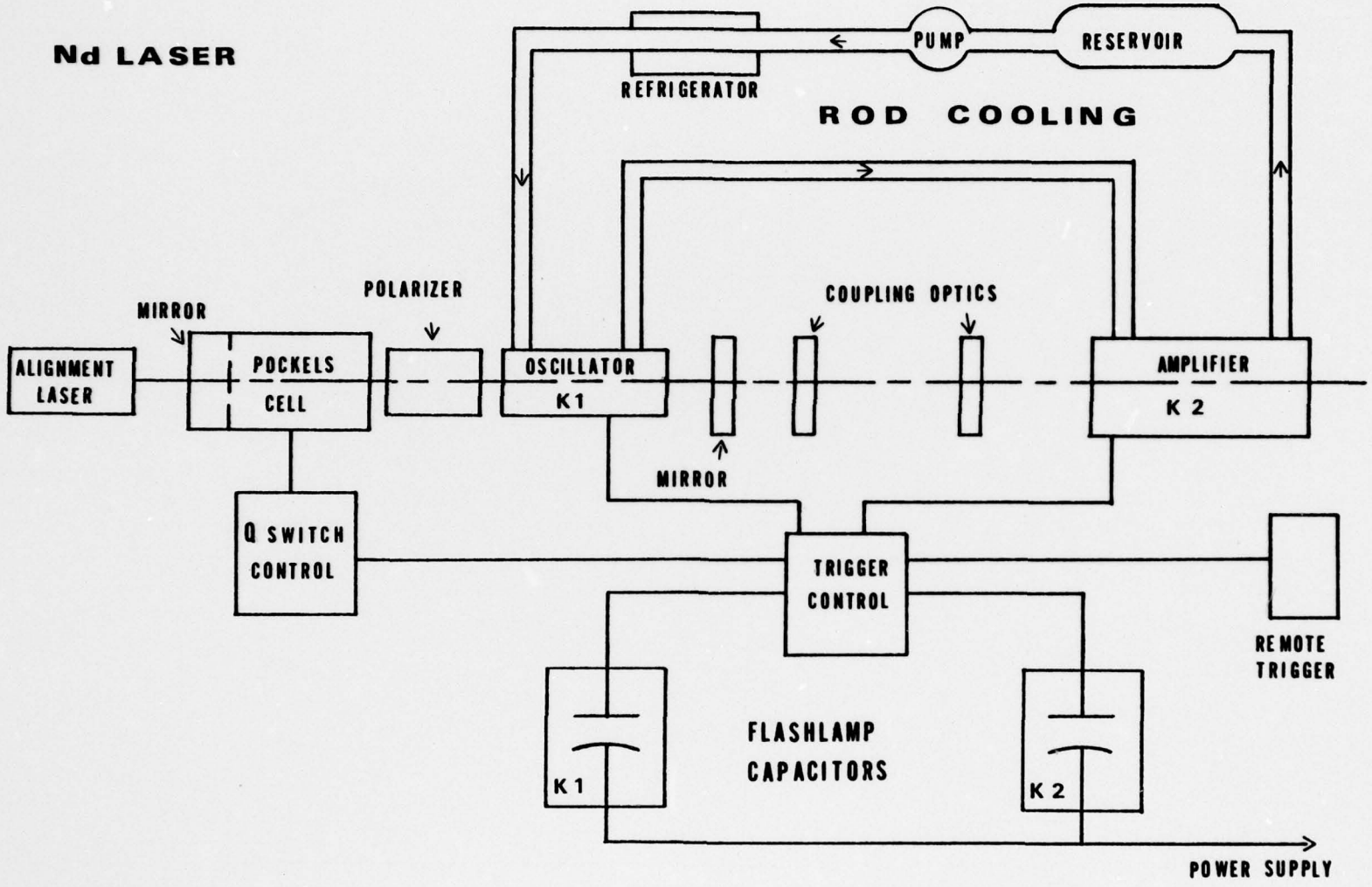

Figure 8 - THE LASER SYSTEM

APPENDIX B

THE TEST CHAMBER

The test chamber subsystem consisted of the main chamber, a mass spectrometer, the vacuum system, a gas bleed system, and various gauges and meters.

A. MAIN CHAMBER

The main vacuum chamber used was one that had been previously used for laser generated plasma experiments conducted at the Naval Postgraduate School. Although this chamber was not bakeable and was limited by o-ring seals and installed pumps to a vacuum of the order of 10^{-7} Torr, it was selected on the basis of economy and convenience since it was adapted to the configuration of the KORAD Nd laser space at the laboratory. The chamber was machined in the shape of an assymetrical octagon from a block of commercial grade aluminum. The volume of the entire vacuum chamber including the mass spectrometer was 12.9±.3 liter. A schematic of the entire experimental arrangement is given in Fig. 3. Two views of the chamber are given in Fig. 9.

There were a total of seven ports provided in the side walls of the chamber and one in the top. The mass spectrometer was mounted to one of the side ports. Another was used to mount an electrical feed through connection for

a thermocouple. A window transparent to 1.06 micrometer radiation was mounted in a third side port to act as an optical feedthrough for the laser light. Pyrex glass plates covered the rest of the side ports to serve as observation windows. The one large port in the top was also covered with a Pyrex plate. This port was used as an access for changing targets. All glass plates and flanges covering these ports were sealed with rubber o-rings.

There were three valves connected to the chamber. A flanged gate valve provided isolation from the diffusion pump. A soldered globe valve cut off the chamber from the forepump roughing system. A small globe valve isolated the gas bleed system. No valve was provided between the chamber and the mass spectrometer.

The two final attachments to the main chamber were an ion gauge and a rotating feedthrough. The rotating feedthrough allowed for mounting the target disks inside the chamber by screwing them onto the threaded end of the feedthrough rod. The geometry was such that the laser beam struck the target at an angle of 30° to its surface normal and that the mass spectrometer was directly opposite to the target surface.

B. MASS SPECTROMETER

Mass spectrometric measurements were made with a Varian Partial Pressure Gauge Mod. 974-0035 [38]. The mass spectrometer gauge had a separate controller which allowed operation in either a total pressure or in a partial pressure mode. The partial pressures were detected for specific charge to mass ratios. The controller also allowed automatic sweeps of partial pressure in two mass ranges or

manual selection of a partial pressure peak for a single charge to mass ratio. Thus, for different species with the same charge to mass ratio such as N_2^+ and CO^+, the contributions of the individual species to the partial pressure reading could not be distinguished. The partial pressure collectors were arranged to detect either in the 1-10 AMU or in the 10-70 AMU mass range. The detectable partial pressure range was 5×10^{-6}-2×10^{-11} Torr. A maximum operating total pressure was 1×10^{-4} Torr.

C. VACUUM SYSTEM

The vacuum pumping system consisted of a SPEEDIVAC ED500 mechanical forepump and a VEECO EP4W oil diffusion pump with a liquid nitrogen cold trap. The forepump had a capability of bringing the entire system down to about 10^{-3} Torr. The diffusion pump with a charged cold trap could reduce the chamber pressure to about 10^{-7} Torr. The rated pumping speed of the diffusion pump was 425 liter/second. A complete checklist for startup and shutdown of the vacuum system is given by Callahan [37].

D. GAS BLEED SYSTEM

The gas bleed in system as shown in Fig. 3 and in Fig. 9 consisted of a tank of commercial grade compressed

gas, a pressure regulator, plastic supply line, a needle valve for fine control of gas pressure, and a cut off isolation valve mounted on the chamber. The system was also provided with an atmospheric vent to allow venting of the chamber and purging of the supply line. To flood the chamber with a test gas, the system was pressurized, allowed to purge through the vent valve, and then admitted slowly into the chamber by cracking open the cut off valve. The pressure was then maintained at the desired level by operating the needle valve. The chamber was not isolated from the pumps for this procedure.

E. GAUGES AND RECORDERS

The total pressure inside the vacuum chamber was monitored with an ion gauge mounted in the lower part of the chamber (see Fig. 9). This was a Hughes 6578 hot cathode type tube. The pressure range was 1 micron to 2×10^{-9} Torr. A Granville-Phillips series 236 Mod 02 controller was used with this tube. The total pressure signal was recorded on a Houston OMNIGRAPHIC Mod HR-96 X-Y recorder. The pressure signal was fed into the Y input and the X input was set to sweep at .01 inches per second.

The partial pressure signal from the mass spectrometer was fed into a Varian G-14 strip recorder. This recorder had two horizontal sweep speeds and a variable vertical deflection scale. For this experiment the recorder was set at the fast speed of .25 inches per second.

The ambient temperature at the rear of the target was monitored with a copper-constantan thermocouple. The wire was passed through an electrical feedthrough to a Doric

Trendicator 400A meter. This meter had a digital readout calibrated to the nearest 0.1°C. No automatic recording was provided for the temperature. The meter was read immediately after each laser pulse which struck the target.

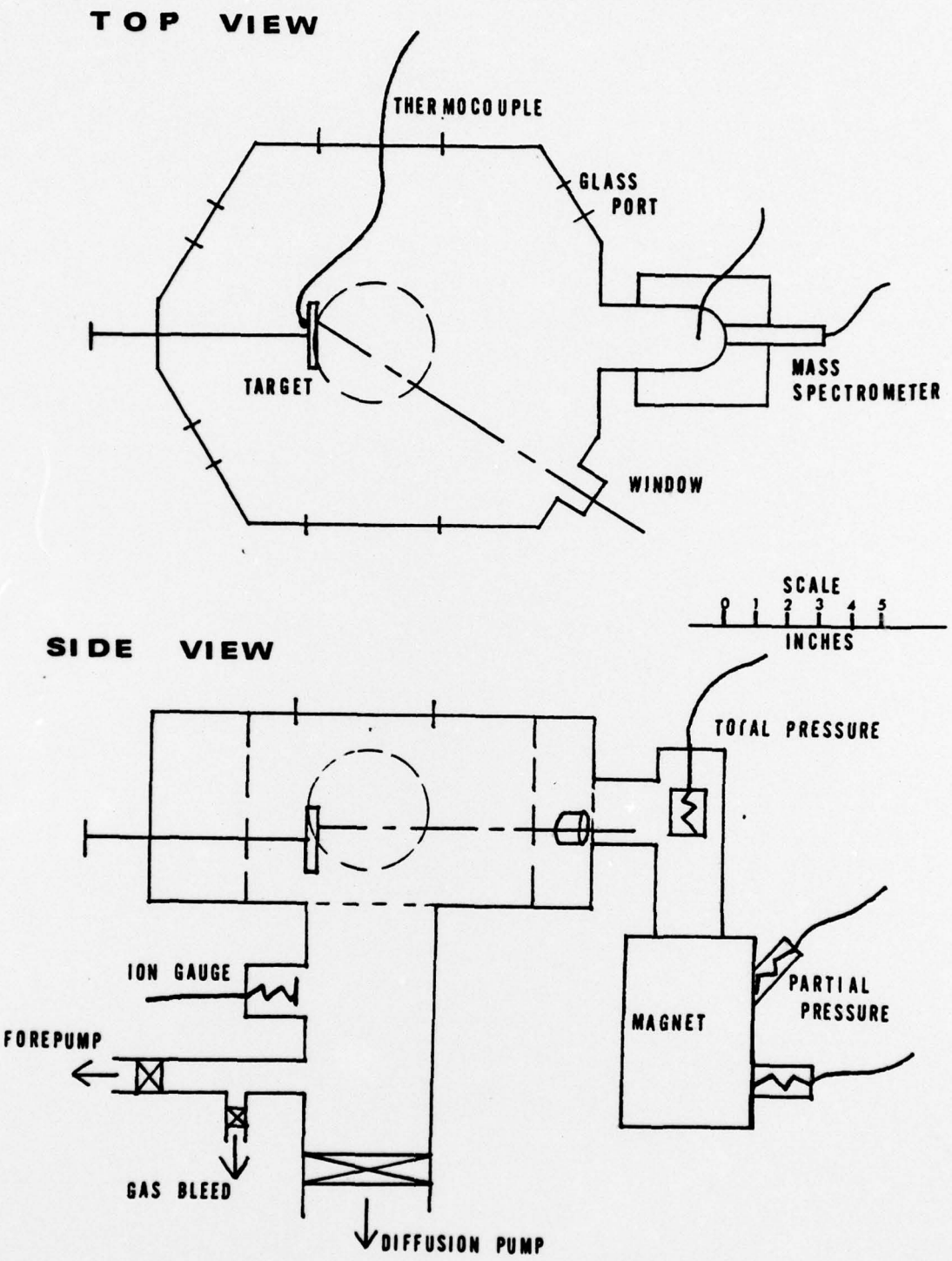

Figure 9 - THE VACUUM CHAMBER

LIST OF REFERENCES

1. Lichtman, D. and McQuistan, R.B., " Slow Electron Interaction with Adsorbed Gases", Progress in Nuclear Energy, series IX, v. 4, p. 93-136, 1965.

2. Bedair, S.M. and Smith, H.P., Jr., " Atomically Clean Surfaces by Pulsed Laser Bombardment", J. of Applied Physics, v. 40, p. 4776-4781, 1969.

3. Peavey, J. and Lichtman, D., " Photon Induced Desorption Using Synchroton Radiation", Surface Science, v. 27, p. 649-652, 1971.

4. Fabel, G., Cox, S., and Lichtman, D., " Photo-desorption from 304 Stainless Steel", Surface Science, v. 40, p. 571-582, 1973.

5. McAllister, J.W. and White, J.M., " Photodesorption of Carbon Monoxide from Polycrystalline Nickel", J. of Chemical Physics, v. 58, p. 1496-1504, 1973.

6. Adams, R.O. and Donaldson, E.E., " Photodesorption", J. of Chemical Physics, v. 42, p. 770-774, 1965.

7. Levine, L.P., Ready, J.F., and Bernal, E., " Gas Desorption Produced by a Giant Pulse Laser", J. of Applied Physics, v. 38, p. 331-336, 1967.

8. Chen, J.M. and Chang, C.C., " Laser Desorption of Submonolayers of Na and Cs from Ge Substrates", J. of Applied Physics, v. 43, p. 3884-3886, 1972.

9. Schwirzke, F., Brinkschulte, and Hashmi, M., " Laser-Induced Desorption of Gas from Metallic Surfaces", J.

of Appl. Physics, v. 46, p. 4891 - 4894, 1975.

10, Brumbach, S. and Kaminsky, M., "X-ray Impact Induced Desorption of Gases from Surfaces", Paper presented at 2nd International Conference on Surface Effects in Controlled Fusion Devices, San Francisco, California, February 16-20, 1976.

11. Young, D. M. and Crowell, A. D., Physical Adsorption of Gases, p. 1-171, Butterworths, 1962.

12, Menzel, D., "Desorption Phenomena", Topics in Applied Physics, vol. 4, p. 101-142, ed. by R. Gomer, Springer-Verlag, New York, N. Y., 1975.

13. Dash, J.G., Films on Solid Surfaces, p. 5-32, Academic Press, New York, N.Y., 1975.

14. Adamson, A. W., Physical Chemistry of Surfaces, 2nd Edition, p. 263-312 and 537-644, Interscience, 1967..

15, Flood, E.A., The Solid Gas Interface, vol. 1 and 2, Marcel Dekker, Inc., New York, N.Y., 1966.

16. Langmuir, I., " The Adsorption of Gases on Plane Surfaces of Glass, Mica and Platinum", J. American Chemical Society, v. 40, p. 1361-1402, 1918.

17. Fowler, R.H., " Adsorption Isotherms. Critical Conditions", Proc. Camb. Phil. Society, v. 32, p. 144-151, 1936.

18, Brunauer, S., The Adsorption of Gases and Vapors, vol. 1, Princeton University Press, Princeton, N.J., 1945.

19. Brunauer, S., Emmett, P., and Teller, E., " Adsorption of Gases in Multimolecular Layers", J. American Chemical Society, v. 60, p. 309-319, 1938.

20. Gomer, R., "Chemisorption", Fundamentals of Gas-Surface Interactions, p. 182-215, ed. Saltsburg, Smith and Rogers, Academic Press, New York, N.Y., 1967.

21. Becker, J.A. and Hartman, C.D., " Field Emission Microscope and Flash Filament Techniques for the Study of Structure and Adsorption on Metal Surfaces", J. of Physical Chemistry, v. 57, p. 153-159, 1953.

22. Ehrlich, G., " Kinetic and Experimental Basis of Flash Desorption", J. of Appl. Physics, v. 32, p. 4-15, 1961.

23. Redhead, P.A., " Thermal Desorption of Gases", Vacuum, v. 12, p. 203-211, 1962.

24. Lange, W.J., " Photodesorption of Carbon Monoxide", J. of Vacuum Science and Technology, v. 2, p. 74-79, 1965.

25. Lange, W.J. and Riemersma, H., " Desorption of Gas by Photons", American Vacuum Society Transactions of the Eighth National Vacuum Symposium, v. 1, p. 167-170, 1961.

26. Terenin, A. and Solonitzin, Yu., " Action of Light on the Gas Adsorption by Solids", Discussions of the Faraday Society, v. 28, p. 28-35, 1959.

27. Kronauer, P. and Menzel, D., "Photodesorption of Carbon Monoxide from Tungsten", Adsorption-Desorption Phenomena, p. 313-328, ed. Ricca, Academic Press, New York, N.Y., 1972.

28. Menzel, D. and Gomer, R., " Desorption from Metal Surfaces by Low-Energy Electrons", J. of Chemical Physics, v. 41, p. 3311-3328, 1964.

29. Bechtel, J. H., " Heating of Solid Targets with Laser

Pulses", J. of Appl. Physics, v. 46, p. 1585-1593, April 1974.

30. Schriempf, J. T., Response of Materials to Laser Radiation: A Short Course, p. 7-21 and 22-40, Naval Research Laboratory Report 7728, 1974.

31. Fuhs, A.E. and Fuhs, S.E., " Computer-drawn Graphs Help Calculate Effects of Heating by Laser Radiation", Laser Focus, v. 12, no. 6, p. 66-73, 1976.

32. Ready, J. F., Effects of High Power Laser Radiation, p. 67-82; 114-116;127-161; 317-358, Academic Press, 1971.

33, American Society for Metals, Metals Handbook, vol. 1, 8th Edition, ASM, Novelty, Ohio, 1961.

34, Union Carbide Electronics, KORAD Laser Systems Instruction Manual for Nd:glass Laser, five volumes, KORAD Dept., Santa Monica, California, 1969

35. Maiman, T. H., " Optically Pumped Solid State Lasers", Solid State Design, v. 4, p. 17-21, 1963.

36. Davis, L. J., Self-Generated Magnetic Fields Produced by Laser Bombardment of a Solid Target, p. 14-30, M. S. Thesis, U. S. Naval Postgraduate School, Monterey, California, 1971.

37. Callahan, D. J., Laser Plasma Particle Velocities , p. 79-103, M. S. Thesis, U. S. Naval Postgraduate School, Monterey, California, 1976.

38, Varian Associates, Partial Pressure Gauge Mod. 971-0035 and Control Unit Mod. 974-0036 Instruction Manual, Vacuum Division, Palo Alto, California, 1966.

INITIAL DISTRIBUTION LIST

		No. Copies
1.	Defense Documentation Center Cameron Station Alexandria, Virginia 22314	2
2.	Library, Code 0212 Naval Postgraduate School Monterey, California 93940	2
3.	Department Chairman, Code 61 Department of Physics and Chemistry Naval Postgraduate School Monterey, California 93940	1
4.	Assoc Professor F. R. Schwirzke, Code 61Sw Naval Postgraduate School Monterey, California 93940	3
5.	Professor A. W. Cooper, Code 61Cr Naval Postgraduate School Monterey, California 93940	1
6.	LCDR J.S. Polk, USN USS Paul F. Foster (DD 964) FPO San Francisco, California 96601	1